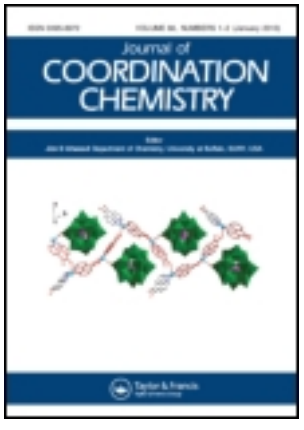

Journal of Coordination Chemistry
Publication details, including instructions for authors and subscription information:
http://www.tandfonline.com/loi/gcoo20

DNA interactions, photocleavage, and cytotoxicity of fluorescein-porphyrinatozinc complexes with different lengths of links

Jiazheng Lu [a], Xiangwen Liao [a], Bin Wu [b], Ping Zhao [c], Jing Jiang [a] & Yongli Zhang [d]

[a] Chemistry Department, School of Pharmacy, Guangdong Pharmaceutical University, The Pepoles' Hospital of Shiling Huadu, Guangzhou, P.R. China

[b] Guangzhou, P.R. China

[c] School of Medicine Chemistry and Chemical Engineering, Guangdong Pharmaceutical University, Guangzhou, P.R. China

[d] School of Basic Courses, Guangdong Pharmaceutical University, Guangzhou, People's P.R. China

Accepted author version posted online: 18 Mar 2013.Published online: 19 Apr 2013.

To cite this article: Jiazheng Lu, Xiangwen Liao, Bin Wu, Ping Zhao, Jing Jiang & Yongli Zhang (2013) DNA interactions, photocleavage, and cytotoxicity of fluorescein-porphyrinatozinc complexes with different lengths of links, Journal of Coordination Chemistry, 66:9, 1574-1590, DOI: 10.1080/00958972.2013.786051

To link to this article: http://dx.doi.org/10.1080/00958972.2013.786051

Journal of Coordination Chemistry, 2013
Vol. 66, No. 9, 1574–1590, http://dx.doi.org/10.1080/00958972.2013.786051

DNA interactions, photocleavage, and cytotoxicity of fluorescein–porphyrinatozinc complexes with different lengths of links

JIAZHENG LU*†, XIANGWEN LIAO†, BIN WU‡, PING ZHAO*§, JING JIANG† and YONGLI ZHANG¶

†Chemistry Department, School of Pharmacy, Guangdong Pharmaceutical University, Guangzhou, P.R. China
‡The Pepoles' Hospital of Shiling Huadu, Guangzhou, P.R. China
§School of Medicine Chemistry and Chemical Engineering, Guangdong Pharmaceutical University, Guangzhou, P.R. China
¶School of Basic Courses, Guangdong Pharmaceutical University, Guangzhou, People's P.R. China

(*Received 25 May 2012; in final form 10 January 2013*)

Three fluorescein–porphyrinatozinc complexes Zn(Fl-PPTPP) (**1**) (Fl-PPTP*p* = 5-(4-fluoresceinpropyloxy)phenyl-10,15,20-triphenylporphyrin), Zn(Fl-HPTPP) (**2**) (Fl-HPTP*p* = 5-(4-fluoresceinhexyloxy) phenyl-10,15,20-triphenylporphyrin) and Zn(Fl-DPTPP) (**3**) (Fl-DPTP*p* = 5-(4-fluorescein decoxy) phenyl-10,15,20-triphenylporphyrin) have been synthesized and characterized by elemental analysis, IR, UV/Vis, Electrospray mass spectra, and ^{1}H NMR. The DNA-binding behaviors of these complexes with calf-thymus DNA (CT-DNA) were investigated by UV–vis absorption titration, fluorescence spectra, viscosity measurements, thermal denaturation, and circular dichroism. The results suggest that **1**, **2**, and **3** interact with CT-DNA by intercalation, and the conformation of fluorescein–porphyrin hybrids is an important factor affecting the DNA-binding affinities. The DNA-binding affinities (K_b values) follow the order **1** > **2** > **3**. In addition, their photocleavage reactions with pBR322 supercoiled plasmid DNA were investigated by gel electrophoresis. All complexes exhibit significant DNA cleavage activity. These complexes have cytotoxic activities against myeloma cell (Ag8.653) and gliomas cell (U251) lines. Complex **1** was the most potent antitumor agent among the three complexes.

Keywords: Fluorescein; Porphyrinatozinc; Cytotoxicity; DNA-binding; Photocleavage

1. Introduction

Interaction of transition metal complexes with DNA has importance in designing new and promising drugs, probes for nucleic acids, DNA-dependent electron transfer reactions, DNA footprinting, sequence-specific cleaving agents, and antitumor drugs [1–3]. Porphyrins and metallo-porphyrins have been used in light-activated cancer treatment photodynamic therapy (PDT), in sensor design due to their fluorescent and electrochemical properties and in gene therapy because of their special photophysical and electrochemical

*Corresponding authors. Email: lujia6812@163.com (J. Lu); zhaoping666@163.com (Z. Zhao).

properties, remarkable stability, and well-known structure [2–4]. They could be selectively taken up by tumor cells and have been used as tumor targeting agents in PDT [5,6]. PDT, in which light activates a photosensitizing drug and elicits the $^1O_2$ mediated cytotoxic action, has recently emerged as a promising modality against cancer and allied diseases [7, 8].

Porphyrins are one of the most studied DNA-binding agents and the interaction of porphyrin with DNA has been extensively studied [9–13]. In fact, porphyrin derivatives, depending on their structure, and the presence of coordinated metal including possible axial ligands, display different preferences not only for binding modes, but also for different DNA sequences. Binding may be either intercalative or external, in the minor groove (in some special cases with self-stacking), depending on the charge distribution of the porphyrin presence and the type of metal in the porphyrin and on the peripheral substituents [7, 14–16]. The development of new photoactive, intercalating moiety in conjunction with the porphyrin chromophore might accentuate the photochemical activity of the derived hybrid molecules, which may lead to efficient DNA binding and DNA cleavage [17–19]. In the pursuit of improved stability and high DNA binding, design of new complexes remains an important challenge. Among the various non-porphyrinic chromophores that can be linked to the porphyrin in such new hybrids, fluorescein seemed an ideal candidate because it is a ubiquitous electron acceptor [20–23]. In earlier work, we have synthesized three fluorescein–porphyrinatozinc complexes Zn(Fl-HPTTP) (Fl-HPTT*p* = 5-(4-fluoresceinhexyloxy)phenyl-10,15,20-tritoylporphyrin), Zn(Fl-HPTPP) (Fl-HPTP*p* = 5-(4-fluoresceinhexyloxy)phenyl-10,15,20-triphenylporphyrin) and Zn(Fl-HPTCPP) (Fl-HPT CP*p* = 5-(4-fluoresceinhexyloxy)phenyl-10,15,20-tri(4chloro)phenylporphyrin), and studied their DNA-binding behaviors and their photocleavage reactions with pBR322 supercoiled plasmid DNA [23]. The results suggest that DNA binding affinities of these fluorescein–porphyrinatozinc(II) complexes may be closely associated with the electronic effects of the substituent group introduced on the porphyrin.

As a systematic study of these molecules and to know whether the length of the flexible long alkoxy chain between fluorescein group and porphyrin hybrid affects DNA-binding affinities of these complexes, we report the synthesis and characterization of three fluorescein–porphyrinatozinc complexes Zn(Fl-PPTPP) (**1**) (Fl-PPTP*p* = 5-(4-fluoresceinpropyloxy)phenyl-10,15,20-triphenylporphyrin), Zn(Fl-HPTPP) (**2**) (Fl-HPTP*p* = 5-(4-fluoresce inhexyloxy)phenyl-10,15,20-triphenylporphyrin), and Zn(Fl-DPTPP) (**3**) (Fl-DPTP*p* = 5-(4-fluoresceindecoxy)phenyl-10,15,20-triphenylporphyrin), Scheme 1. The interactions of these three complexes with calf-thymus DNA (CT-DNA) were investigated using UV–vis absorption titration, fluorescence spectra, viscosity measurements, thermal denaturation and

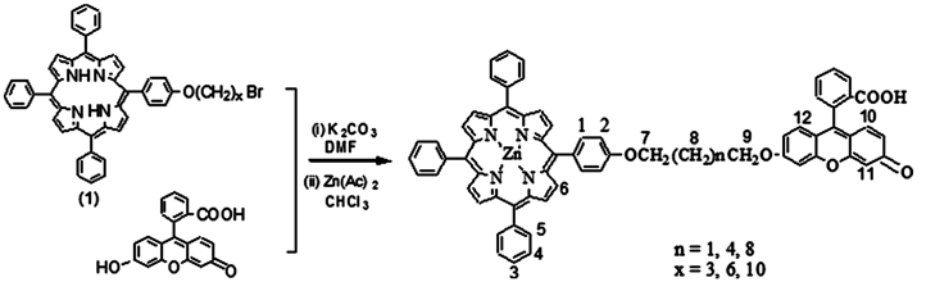

Scheme 1. Synthesis of fluorescein-porphyrinatozinc(II) complexes. (**1**): $x = 3$, $n = 1$; (**2**): $x = 6$, $n = 4$; (**3**): $x = 10$, $n = 8$.

circular dichroism (CD). The effect of fluorescein–porphyrinatozinc complexes conformation has been discussed. Their photocleavage reactions with pBR322 supercoiled plasmid DNA were investigated by gel electrophoresis. In addition, the cytotoxicity of these three complexes against the myeloma cell (Ag8.653) and gliomas cell (U251) were assessed by MTT (3-(4,5-dimethylthiazoyl-2-yl)2,5-diphenyltetrazoliumbromide) assay.

2. Experimental

2.1. *Materials and methods*

$CHCl_3$ and other chemicals used in the synthesis and physical measurements were purified prior to use by published methods [21–23].

Disodium salt of calf thymus DNA (Sigma) was used as received. A solution of CT-DNA in buffer I gave a ratio of UV absorbance at 260 and 280 nm of 1.8–1.9 : 1, indicating that the DNA was sufficiently free of protein [23–26]. The DNA concentration per nucleotide was determined by absorption spectroscopy using the molar absorption coefficient (6600 $(ML^{-1})^{-1}\,cm^{-1}$) at 260 nm [7,15,24]. Stock solutions were stored at 4 °C and used after no more than 3 days. PBR 322 DNA was also purchased from Sigma and used without purification. Other materials were analytical reagent grade and used without purification unless otherwise noted.

Buffer I, 5 mML^{-1} Tris–HCl/50 mML^{-1} NaCl in water (pH 7.0) was used for absorption titration, fluorescence spectra, viscosity measurements, thermal denaturation and CD. Buffer II, 50 mML^{-1} Tris–HCl/18 mML^{-1} NaCl in water (pH 7.2) was used for DNA-binding studies and gel electrophoresis experiments. Buffer III, Tris–boric acid–EDTA in water (pH 8.3) was used for gel electrophoresis experiments. A phosphoric acid buffer containing 1.5 mML^{-1} Na_2HPO_4, 0.5 mML^{-1} NaH_2PO_4 and 0.25 mML^{-1} Na_2H_2EDTA (H_4EDTA=N, N′-ethane-1,2-diylbis[N-(carboxymethyl)glycine]) (pH 7.0) was used for thermal denaturation. Compounds were dissolved in DMSO and diluted with buffer solution to the required concentrations prior to use.

2.2. *Physical measurements*

Microanalyses (C, H, and N) were carried out with a Perkin-Elmer 240Q elemental analyzer. Electrospray mass spectra (ES-MS) were recorded on a LCQ system (Finnigan MAT, USA) using methanol as mobile phase. ^1H NMR spectra were recorded on a Varian-500 spectrometer. All chemical shifts are given relative to tetramethylsilane. Infrared spectra were recorded on a Bomen FTIR model MB102 instrument using KBr pellets. UV–vis spectra were recorded on a Shimadzu UV-3101 PC spectrophotometer at room temperature. Emission spectra were recorded on a Perkin-Elmer Lambda 55 spectrofluorophotometer. CD spectra were recorded on a JASCO-J810 spectrometer.

2.3. *DNA interactions*

The absorption titration of fluorescein–porphyrinatozinc(II) complexes in Tris–HCl buffer was performed by using a fixed concentration of the fluorescein–porphyrinatozinc(II) complex (20 μML^{-1}) to which the DNA stock solution was added. Fluorescein–Porphyrinatozinc(II)-DNA solution was allowed to incubate for 3 min before the absorption

spectra were recorded. To elucidate the binding strength of the complex, the intrinsic binding constant K_b with CT-DNA was obtained by monitoring the change in absorbance of the ligand transfer band with increasing amounts of DNA. The intrinsic binding constant K_b of the complex to DNA was calculated by using the following equation [24–27]:

$$\frac{[\mathrm{DNA}]}{\varepsilon_a - \varepsilon_f} = \frac{[\mathrm{DNA}]}{\varepsilon_b - \varepsilon_f} + \frac{1}{K_b(\varepsilon_b - \varepsilon_f)}$$

where [DNA] is the concentration of DNA in base pairs, ε_a, ε_f and ε_b refer to the corresponding apparent absorption coefficient A_{obsd}/[Zn(Fl-Por)], the extinction coefficient for the free fluorescein–porphyrinatozinc(II) complex and the extinction coefficient for the fluorescein–porphyrinatozinc(II) complex in the fully bound form, respectively. In plots of $[\mathrm{DNA}]/(\varepsilon_a - \varepsilon_f)$ *versus* [DNA], K_b is obtained by the ratio of slope to intercept.

Viscosity measurements were carried out using an Ubbelohde viscometer maintained at 28 ± 0.1 °C in a thermostatic bath. Flow time was measured with a digital stopwatch, and each sample was measured five times to obtain the average flow time. Data were presented as $(\eta/\eta_0)^{1/3}$ *versus* binding ratio [16, 22–26], where η is the viscosity of DNA in the presence of complexes, while η_0 is the viscosity of DNA alone. Viscosity values were calculated from the observed flow time of DNA-containing solution ($t > 100$ s) corrected for the flow time of buffer alone (t_0), $\eta = (t - t_0)/t_0$ [24–26].

Thermal denaturation studies were carried out with a Shimadzu UV-3101 PC spectrophotometer equipped with a Peltier temperature-controlling programmer (±0.1 °C). The melting curves were obtained by measuring the absorbance at 260 nm for solutions of CT-DNA (100 μML^{-1}) in the absence and presence of different concentrations of fluorescein–porphyrinatozinc(II) complexes as a function of temperature. The temperature was scanned from 40 to 92 °C at 1 °C min^{-1}. The melting temperature (T_m) was taken as the midpoint of the hyperchromic transition.

The CD spectra of **1**, **2**, and **3** in the absence and presence of CT-DNA were performed on a JASCO-J810 spectrometer by using a fixed concentration of fluorescein–porphyrinatozinc(II) complex [Zn(Fl-Por)] = 10 μML^{-1}, and [DNA] = 120 μML^{-1}, respectively. The spectra were recorded at 25 °C after samples had been incubated with CT-DNA for 24 h at 37 °C.

2.4. *Photo-induced cleavage of pBR 322 DNA by fluorescein–porphyrinatozinc(II) complexes*

For the gel electrophoresis experiments, pBR322 supercoiled plasmid DNA 0.5 μL (100 μML^{-1} DNA-nucleotide) in Tris-HCl buffer (pH 7.2) was treated with 1.0 μML^{-1} fluorescein–porphyrinatozinc(II) complex dissolved in DMSO. The mixture was incubated for 30 min and then irradiated with a high-pressure mercury lamp (irradiation at 365 nm, 40 W, 25 cm above the solution surface) at room temperature for 60 min, then with white-light including 350 nm (fluorescein absorption) and 420 nm (porphyrin absorption, 25 mW cm^{-2}). The samples were analyzed for 30 min at 40 V in Buffer III containing 1% agarose gel. The gel was stained using 1.0 mg mL^{-1} ethidium bromide (EB) and photographed under UV light.

2.5. *Cytotoxicity studies in vitro*

2.5.1. Cytotoxicity assays. The capacities of compounds to interfere with the growth of myeloma cells (Ag8.653) and gliomas cells (U251) were determined by MTT dye assay. Compounds were dissolved in DMSO and diluted with Sera Free Cryopreservation Media (RPMI) 1640 to the required concentrations prior to use. The control well was prepared by addition of culture medium (100 μL). Wells containing culture medium without cells were used as blanks. Myeloma cells (Ag8.653) and gliomas cells (U251) with a density 2×10^4 cells per well were precultured into 96-well microtiter plates for 48 h at 37 °C with 5% CO_2. Upon completion of the incubation, stock MTT dye solution was added to each well. After 4 h incubation, a solution containing N,N-dimethylformamide (50%) sodium dodecyl sulfate (20%) was added to solubilize the MTT formazan. The cell viability was determined by measuring the absorbance of each well at 490 nm using a Multiskan SSCENT microplate reader. IC_{50} values were determined by plotting the percentage viability *versus* concentration on a logarithmic graph and reading off the concentration at which 50% of cells remain viable relative to the control.

2.5.2. Cell cycle analysis. Cell cycle of control and treated cancer cells were determined. Using standard methods, the DNA of cells were stained with propidium iodide (PI) and the proportion of non-apoptotic cells in different phases of the cell cycle recorded. The cancer cells were treated with the complex, harvested by centrifugation at $1000 \times g$ for 5 min and then washed with ice-cold phosphate buffer solution (PBS). The collected cells were fixed overnight with cold 70% ethanol and then stained with PI solution consisting of 50 μg mL^{-1} PI, 10 μg mL^{-1} RNase. After 10 min incubation at room temperature in the dark, fluorescence-activated cells were sorted in a FACScan flow cytometer using Cell Quest 3.0.1 software. The percentage of cells in each phase of the cell cycle was determined as least in triplicate and expressed as mean ± SD.

2.6. *Preparation of complexes*

The zinc(II) complex, Zn(Fl-PPTPP) **(1)** was synthesized with a method similar to that described earlier (see scheme 1) [19,21–23]. A mixture of Fl-PPTPP (105 mg), $Zn(OAc)_2$ (1.1 g), $CHCl_3$ (30 cm^3), and HOAc (20 cm^3) was first stirred for 5 min at room temperature. Then, the reaction mixture was maintained under reflux for 3 h at 60 °C. After this, the mixture was diluted with another 20 cm^3 $CHCl_3$ and washed with water (6×50 cm^3). Then, it was dried with anhydrous Na_2SO_4 and concentrated via rotary evaporation. The residue was then chromatographed on a silica gel column using $CHCl_3 : CH_3OH = 18 : 1$ (*V/V*) mixture as eluent, yielding a purple solid. The yield of Zn(Fl-PPTPP) was 90.6%. Anal. Found: C, 75.2; H, 4.0; N, 5.0; Calcd for $C_{67}H_{44}N_4O_6Zn$: C, 75.5; H, 4.2; N, 5.3%. ^1H NMR (500 Hz, DMSO, ppm): δ 11.15 (s, 1H, COOH), 8.84–8.72 (m, 8H, 6-H), 8.19–8.32 (d, 6H, d, $J = 7.8$ Hz, 4-H), 8.17–8.16 (d, 2H, $J = 4.2$ Hz, 2-H), 7.80–7.90 (m, 11H 1,3,5-H), 7.50–7.53 (d, 4H, $J = 8.7$ Hz, phenyl ring-H), 6.88–7.19(m, 6H, 10,11,12-H), 3.23–3.33 (t, 2H, $J = 7.4$ Hz, 7-H), 2.50 (t, 2H, $J = 4.6$ Hz, 8-H), 1.92 (t, 2H, $J = 5.2$ Hz, 9-H); IR (KBr, cm^{-1}): 2924–2855 (C–H), 1722.6 (carboxyl, C=O), 1638.6 (C=O), 1594.9, 1462.5 (C=C) and 1250–1218 (Ar–O–C). UV–vis. (CH_2Cl_2, λ_{max} (nm), $\varepsilon((ML^{-1})^{-1}cm^{-1})$) in parentheses: 420 ($1.13 \times 10^5$), 550 ($5.95 \times 10^3$) and 597 ($2.12 \times 10^3$); ESMS (*m/z*): M^+, 1065.37.

Zn(Fl-HPTPP) (**2**) was prepared in a similar way to that of Zn(Fl-PPTPP) except for (Fl-HPTPP) instead of Fl-PPTTP. The yield of Zn(Fl-HPTPP) was 94.3%. Elem. Anal. Found: C, 72.10%; H, 3.55%; N, 6.96%; Calcd for $C_{70}H_{50}N_4O_6Zn$: C, 72.26; H, 3.64; N, 7.02%. ^{1}H NMR (500 Hz, DMSO, ppm): δ 11.16 (s, 1H, COOH), 8.73–8.90 (m, 8H, 6-H), 8.0–8.4 (6H, d, J = 8.2 Hz, 4-H), 7.85–7.96 (d, 2H, J = 7.8 Hz, 2-H), 7.80–7.83 (m, 11H, 1,3,5-H), 7.30–7.55 (d, 4H, J = 8.7 Hz, phenyl ring-H), 6.98–7.23 (m, 6H, 10,11,12-H), 3.25–3.38 (t, 2H, J = 7.8 Hz, 7-H), 2.95 (t, 2H, J = 6.7 Hz, 9-H), 1.90 (m, 8H, J = 6.4 Hz, 8-H); IR (KBr pellets, ν_{max}/cm^{-1}): 2923–2860 (C–H), 1722 (carboxyl, C=O), 1637 (C=O), 1593 (C=C) and 1258–1216 (Ar–O–C) cm^{-1}; UV–vis. (CH_2Cl_2, λ_{max} (nm), ε ((ML^{-1})$^{-1}$cm^{-1})): 420 (1.13×10^5), 551 (5.95×10^3) and 596 (2.12×10^3); ESMS (*m/z*): M$^+$, 1107.30.

Zn(Fl-DPTPP) (**3**) was prepared in a similar way to that of Zn(Fl-PPTPP) except for (Fl-PPTPP) instead of Fl-DPTPP. The yield of Zn(Fl-DPTPP) was 89.3%. Anal. Found: C, 72.45; H, 3.98; N, 6.64. Calcd for $C_{74}H_{58}N_4O_6Zn$: C, 72.80; H, 4.07; N, 6.74%. ^{1}H–NMR (500 Hz, DMSO, ppm): δ 11.10 (s, 1H, COOH), 8.75–8.98 (m, 8H, 6-H), 8.0–8.3 (6H, d, J = 8.2 Hz, 4-H), 7.88–7.95 (d, 2H, J = 7.8 Hz, 2-H), 7.81–7.85 (m, 11H 1,3,5-H), 7.32–7.56 (d, 4H, J = 8.7 Hz, phenyl ring-H), 6.50–7.20 (m, 6H, 10,11,12-H), 3.35–3.45 (t, 2H, J = 7.8 Hz, 7-H), 2.52 (t, 16H, J = 6.7 Hz, 8-H), 1.95 (t, 2H, J = 6.4 Hz, 9-H); IR (KBr pellets, ν_{max}/cm^{-1}): 2920–2857 (C–H), 1730.3 (carboxyl, C=O), 1632.3 (C=O), 1590.6 (C=C) and 1255–1220 (Ar–O–C) cm^{-1}; UV–vis. (CH_2Cl_2, λ_{max} (nm), ε ((ML^{-1})$^{-1}$cm^{-1})): 418 (1.16×10^5), 549 (5.92×10^3) and 595 (2.32×10^3); ESMS (*m/z*): M$^+$, 1163.65.

3. Results and discussion

3.1. *Synthesis and characterization*

Zinc complexes **1**, **2**, and **3** were synthesized by reaction with $Zn(OAc)_2$ in $CHCl_3$ in about 94% yields.

IR spectra clearly indicate the presence of porphyrin and fluorescein with characteristic frequencies of porphyrin and fluorescein observed at 2953–2854 (C–H), 1720 (carboxyl, C=O), 1638.2 (C=O), 1598.3 (C=C) and 1260–1220 (Ar–O–C) cm^{-1}, respectively. A medium intensity N–H band at 3313 cm^{-1} in IR spectra of the ligands was absent in the complexes indicating deprotonation of the porphyrin ring prior to coordination [10,15,22–26].

Electronic spectra of the free-base porphyrins and the new complexes have been recorded in CH_2Cl_2. The spectrum of all metal-free porphyrins has a strong absorption at 420 nm and four other peaks centered at 519, 550, 597, and 646 nm. The peak at 420 nm is the Soret band arising from the $a_{1u}(\pi) - e_g^*(\pi)$ transition and the other four absorptions are attributed to Q bands of the $a_{2u}(\pi) - e_g^*(\pi)$ transition [7, 13, 26, 27]. The fluorescein–porphyrinatozinc(II) complexes show electronic spectra typical of metalloporphyrins. The Q band of zinc complexes in comparison with metal-free ligands has only two absorptions at 550 and 646 nm, typical of porphyrins on going from the metal-free ligands to their Zn complexes. This is due to an increase in the symmetry of the macrocycle, which indicates coordination of porphyrin nitrogen to zinc [10, 21, 27–30].

^{1}H NMR spectra of the metal-free ligands and complexes showed peaks of carboxyl (COOH), alkoxy and phenyl ring-H protons. These indicated that each compound consists of a flexible long alkoxy chain between the fluorescein group and porphyrin with a *carboxyl* at one end. In ^{1}H NMR spectra of **1**, **2,** and **3**, the pyrrole N–H protons (−2.90 ppm) were

not observed, affirming coordination. ^{1}H NMR spectra of **1**, **2,** and **3** are in excellent agreement with the proposed structures as shown in scheme 1.

Assignments of the complexes were also made on the basis of elemental analyses and mass spectral data providing support for the proposed structures. The molecular ion peaks of **1**, **2,** and **3** at *m/z* 1065.40, 1107.30 and 1163.65 (M^+), respectively, were obtained by ESI-MS.

3.2. *DNA interactions*

3.2.1. Electronic absorption titration and fluorescence spectroscopic studies. Electronic absorption spectroscopy is employed to determine the binding of complexes with DNA. Complex bound to DNA through intercalation usually results in hypochromism and red shift (bathochromism), due to the intercalative mode involving a strong stacking interaction between aromatic chromophore and the base pairs of DNA. The extent of the hypochromism is consistent with the strength of intercalative interaction [22–25, 29–32].

In figure 1, absorption spectra of the fluorescein-porphyrinatozinc(II) complexes **1**, **2,** and **3** (at a constant concentration) are shown in the absence and presence of CT-DNA. When CT-DNA was added into porphyrin complexes, hypochromism and red shift are

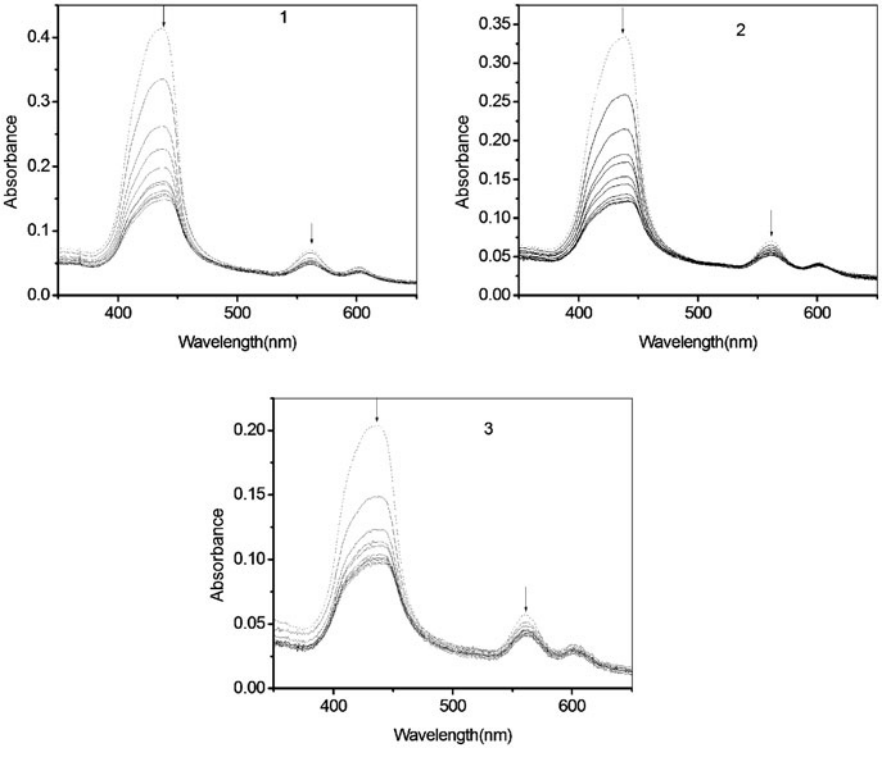

Figure 1. Absorption spectra of **1** (1), **2** (2) and **3** (3) in Tris–HCl buffer upon increasing amounts of CT-DNA. [Zn(Fl-Por)] = 20 μML^{-1}, [DNA] = (0–80) μML^{-1}. Arrows show the absorbance changing upon increasing DNA concentration. λ_{ex} = 420 nm.

Table 1. Change of electronic spectra of **1**, **2,** and **3** in the absence and presence of CT-DNA in 5 mML^{-1} Tris-HCl buffer, 0.1 mML^{-1} NaCl (pH 7.2).

Complex	λ_{max} (free)	λ_{max} (bound)	$\Delta\lambda$/nm	H/%	$K_b/(ML^{-1})^{-1}$
1	420	427	7	24.3	3.52×10^5
	550	553	3	7.2	
2	420	425	5	21.7	3.05×10^5
	550	552	2	7.1	
3	419	423	4	19.8	2.08×10^5
	549	550	1	6.5	

observed at both Soret and *Q* band absorptions for all of these complexes; the data are listed in table 1. Comparing reported results to ours [17, 23–26], we believe that **1**, **2,** and **3** interact with DNA by intercalation, binding with DNA through a stacking interaction between the aromatic chromophore and the base pairs of DNA. In the presence of calf thymus DNA, hypochromism and red shift of **1** are larger than those of **2** and **3**, indicating that the binding affinity of **1** is larger than that of **2** and **3**.

In order to compare quantitatively the binding strength of these complexes with DNA, the intrinsic binding constants K_b were calculated by monitoring the changes of absorbance in the ligand transfer bands, with increasing amounts of CT-DNA (see figure 2). The intrinsic binding constants K_b obtained for **1**, **2,** and **3** were (3.52 ± 0.04), (3.05 ± 0.02) and $(2.08 \pm 0.03) \times 10^5$ $(ML^{-1})^{-1}$, respectively. Such values of intrinsic binding constants indicate that the interaction of **1**, **2,** and **3** with DNA are weaker than previously reported for cationic porphyrin–anthraquinone (Por–AQ) compounds such as 5-[4-[(1-N-anthraquinonon-yl)acetyloxohydroxyl]phenyl]-10,15,20-trisphenylporphyrin (AQATPP) ($K_b = 5.17 \times 10^4$ $(ML^{-1})^{-1}$), 5-[4-(1-N-anthraquinonon-yl)-acetyl-oxophenyl]10,15,20-tris(N-methylpyridinium-4-yl)porphyrin triiodide [AQATMPyP]I_3 ($K_b = 4.9 \times 10^4$ $(ML^{-1})^{-1}$), 5-(4-hydroxyphenyl)-10,15,20-tris(4-N-pyridiniumyl)porphyrin (HTPyP) ($K_b = 6.43 \times 10^4$ $(ML^{-1})^{-1}$), and other systems [5, 9, 14, 16, 24, 25] suggesting that the interaction of **1**, **2,** and **3** with DNA are medium strength intercalation. This may be attributed to higher DNA-binding ability of cations, such as [AQATMPyP]I_3. The anthraquinone moiety in [AQATMPyP]I_3 has more chances to approach the negative DNA unit and thus has more opportunities to interact with DNA bases

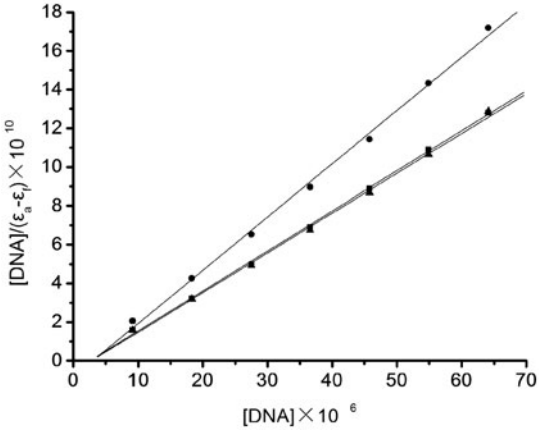

Figure 2. Plots of $[DNA]/(\varepsilon_b - \varepsilon_f)$ *vs.* [DNA] for absorption titration of DNA with the complexes. **1** (●), **2** (■) and **3** (▲), $\lambda_{ex} = 420$ nm.

[16, 23–26]. Meanwhile, these values of intrinsic binding constant also indicate that the interactions of these complexes with DNA are weaker than reported zinc complexes such as [Zn(Mentb)(salicylate)](NO_3) (Mentb = tris(2-(N-methyl)benzimidazylmethyl)amine) [32], [Zn(bpea)Cl_2)] (bpea = N,N-bis(2-pyridylmethyl)ethylamine) [33] and other systems [10, 22, 34]. This difference may be due to the steric hindrance of the fluorescein group. To fully understand the mechanism involved in this difference, further investigation will be needed to carry out.

The K_b decreases in the order **1** > **2** > **3**. The difference lies only in the length of alkoxy chain covalently linking the fluorescein group to the phenyl in the porphyrin ring. Considering the structures of these complexes, we believe the conformations of fluorescein–porphyrinatozinc(II) complexes may be the reason for the difference of their intrinsic binding constants. Since the alkoxy chain that links fluorescein to porphyrin is flexible, a π–π stacking may exist between fluorescein and porphyrin ring in fluorescein–porphyrinatozinc(II) complexes [21–23]. With the increase in the length of alkoxy chain, it is easy to form closed conformation and π–π stacking between fluorescein group and porphyrin ring, decreasing the interaction between the complexes and DNA, resulting in the observed trend in K_b. The results suggest that conformations of fluorescein–porphyrinatozinc(II) complexes may be an important factor affecting DNA binding affinities of these complexes.

Emission spectra of all three complexes in the absence and presence of CT-DNA are shown in figure 3. Upon addition of CT-DNA, the emission intensity increases steadily and becomes 3.56 times larger than that in the absence of DNA for **1**, 3.12 times for **2** and 2.83 times for **3** at the ratio of [DNA]/[Zn(Fl-Por)] = 120. This implies that the complexes intercalate into the base pairs of DNA and are protected by DNA, since the hydrophobic environment provided by DNA can protect them from the accessibility of water molecules and thus prolong the luminescence, leading to an increase of the emission intensity [5–9, 20–24].

According to the Stern–Volmer equation:

$$I/I_0 = 1 + Kr$$

where I_0 and I are the fluorescence intensities in the absence and the presence of fluorescein–porphyrinatozinc(II) complexes, respectively. K is a linear Stern–Volmer quenching constant. r is the ratio of total concentration of DNA to that of fluorescein–porphyrinatozinc(II) complexes. The quenching plots illustrate that the quenching of fluorescein–porphyrinatozinc(II) complexes by DNA is in agreement with the linear Stern–Volmer equation, which also proves that the fluorescein–porphyrinatozinc(II) complexes bind to DNA. With the plot of I/I_0 *versus* [Zn(Fl-Por)]/[DNA], K is given by the ratio of the slope to intercept. The K values for **1**, **2,** and **3** are 16.56 ± 0.23, 13.28 ± 0.15, and 8.67 ± 0.12, respectively, indicating that the interaction of **1** with DNA is the strongest, followed by **2**, and then **3**, consistent with electronic absorption. The K value of **3** is smaller than that of our previously reported for Zn(Fl-HPTTP) (Fl-HPTT*p* = 5-(4-fluoresceinhexyloxy)phenyl-10,15,20-tritolylporphyrin) ($K = 15.6$) and Zn(Fl-HPTCPP) (Fl-HPTCP*p* = 5-(4-fluoresceinhexyloxy)phenyl-10,15,20-tri(4-chloro)phenylporphyrin) ($K = 9.3$) [23]. The difference may be due to the length of alkoxy chain covalently linking the fluorescein group to the phenyl in the porphyrin ring. As stated above, with the increase in the length of alkoxy chain, π–π stacking interaction between fluorescein and porphyrin ring increases. This may decrease the interaction between the complexes and DNA, resulting in the trend in K.

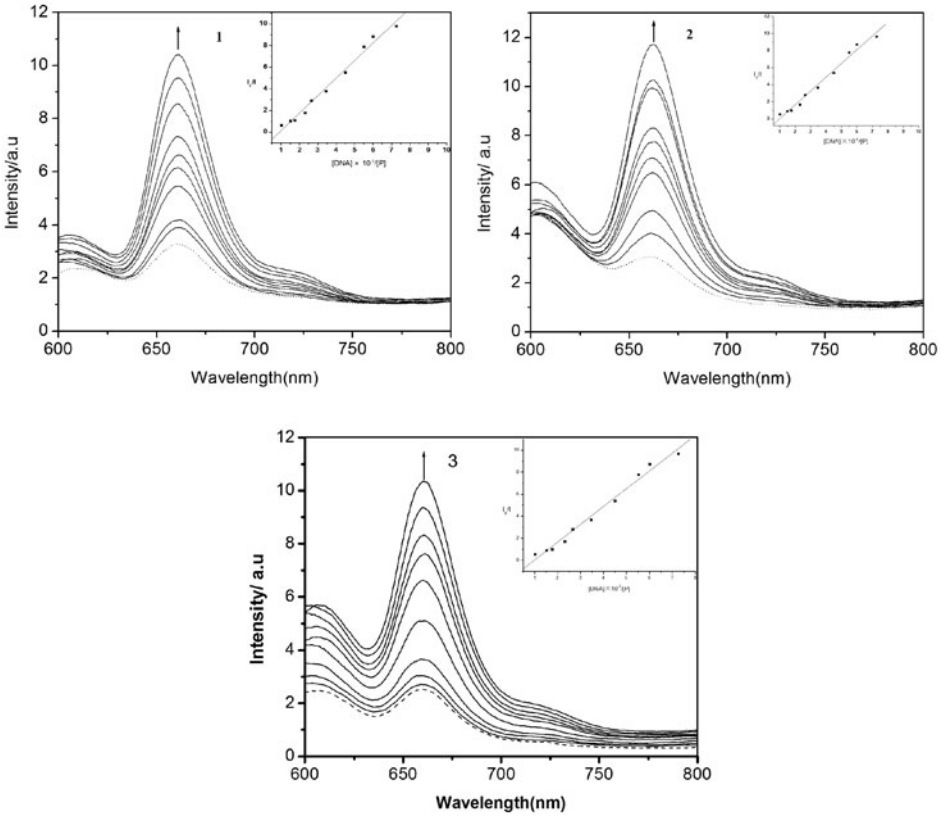

Figure 3. Emission spectra of **1** (1), **2** (2) and **3** (3) in aqueous buffer (Tris 5 mML^{-1}, NaCl 50 mML^{-1}, pH 7.2) at 298 K in the presence (—) and absence (– – –) of CT DNA. Arrows show the intensity changes upon increasing DNA concentration. [Zn(Fl-Por)] = 5×10^{-8} ML^{-1}, λ_{exc} = 420 nm.

3.2.2. Viscosity measurements. To further clarify the binding interaction between both complexes and DNA, viscosity measurements were carried out on CT DNA by varying the concentration of the added complexes. Spectroscopic data are necessary, but not sufficient to support a binding mode. Hydrodynamic measurements that are sensitive to length increase (e.g. viscosity, sedimentation) are regarded as the least ambiguous and the most critical tests of binding in solution in the absence of crystallographic structure data [13, 16, 24–29]. A classical intercalative mode causes a significant increase in viscosity of DNA solution due to increase in separation of base pairs at intercalation sites and hence an increase in overall DNA length. In contrast, a partial, nonclassical intercalation of compounds could bend (or kink) the DNA helix and reduce its effective length and, concomitantly, its viscosity.

The effects of complexes **1**, **2**, **3** and EB on the viscosity of CT-DNA are shown in figure 4. As seen in figure 4, upon increasing the amounts of **1**, **2,** and **3**, the relative viscosity of DNA increases steadily. The increasing degree of viscosity is **1** > **2** > **3**. The viscosity results thus provide strong evidence for intercalation of **1**, **2,** and **3** with DNA.

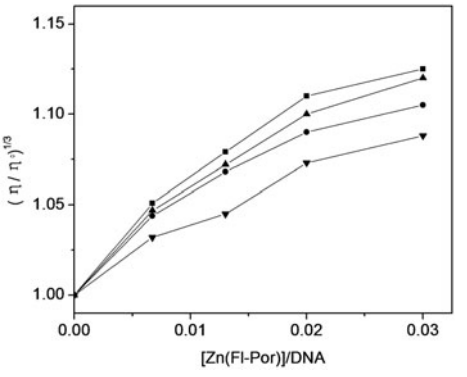

Figure 4. Effect of increasing amounts of EB (■), **1** (▲), **2** (●) and **3** (▼) on the relative viscosities of CT DNA at 25 ± 0.1 °C. The total concentration of DNA is 0.5 mML^{-1}.

3.2.3. Thermal denaturation studies. Thermal behavior of DNA in the presence of compounds can give insight into their conformational changes and offer information about the interaction strength of complexes with DNA. Normally, when the temperature increases, the double-stranded DNA will gradually dissociate to single strands and generate a hyperchromic effect on the absorption spectra of DNA bases ($\lambda_{max} = 260$ nm). The melting temperature T_m, which is defined as the temperature where half of the total base pairs are unbounded, is usually introduced. Generally, T_m will increase considerably when intercalative binding occurs, since intercalation of the complexes into DNA base pairs causes stabilization of base stacking and hence raises the melting temperature of the double-stranded DNA [13, 24, 30, 35].

The melting curves of CT-DNA in the absence and presence of **1**, **2**, and **3** are illustrated in figure 5. The T_m of CT-DNA in the absence of the complexes is 63.4 ± 0.2 °C. As can be seen from figure 5, when mixed with the compounds at a concentration ratio [Zn (Fl-Por)]/[DNA] of 1 : 10, the observed melting temperature in the presence of **1**, **2,** and **3**

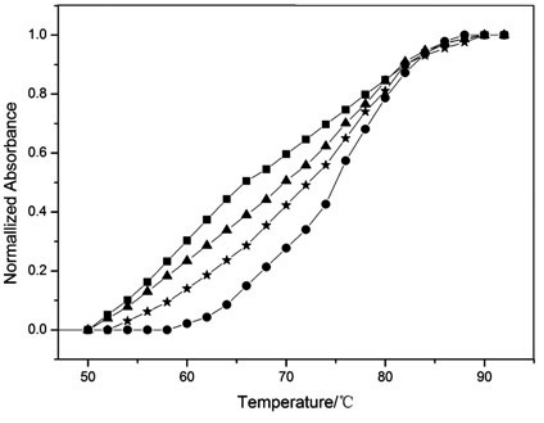

Figure 5. Melting temperature curves of CT-DNA in the absence (■) and presence of **1** (●), **2** (★) and **3** (▲). [Zn(Fl-Por)] = 10 μML^{-1}, [DNA] = 100 μML^{-1}.

reach 72.5 ± 0.2, 69.6 ± 0.2 and 67.7 ± 0.2 °C, respectively. The largest increase of T_m ($\Delta T_m = 9.1$ °C) in the presence of **1**, moderate increase of T_m ($\Delta T_m = 6.2$ °C) in the presence of **2** and smallest increase of T_m ($\Delta T_m = 4.3$ °C) in the presence of **3** are comparable with those observed for classical intercalators and lend strong support for their intercalation with DNA [30–35].

3.2.4. CD spectral studies. CD spectra play an important role in study of the interaction between porphyrin complexes and DNA as CD spectra are very sensitive to binding mode of small molecules to DNA. The sign of the induced CD spectrum of DNA in the Soret region can be used as a sensitive signature for the binding modes of porphyrins to DNA: a positively induced CD band is indicative of external (minor groove) binding, a negatively induced CD band is produced upon intercalation and a conservative induced CD band is the characteristic of outside binding [11, 36–39].

As shown in figure 6, the fluorescein–porphyrinatozinc(II) complexes do not yield CD spectra in the absence of DNA, but CD spectra were induced for the fluoresceinporphyrinatozinc(II) complexes in the presence of DNA, due to the interaction between the transition moments of the achiral porphyrin and chirally arranged DNA base transitions [17, 32–36]. Complexes **1**, **2,** and **3** showed strong negative peaks centered at ca. 440 nm upon binding to calf thymus DNA, suggesting they are excellent DNA intercalators, which further supports the conclusion that **1**, **2,** and **3** interact with CT-DNA by intercalation.

3.3. *Photo-induced cleavage of pBR 322 DNA by fluorescein–porphyrinatozinc(II) complexes*

To further investigate the interactions of these complexes with DNA, photocleavage experiments were employed, in which the cleavage reaction on supercoiled plasmid DNA was monitored by agarose gel electrophoresis. When circular plasmid DNA is subjected to

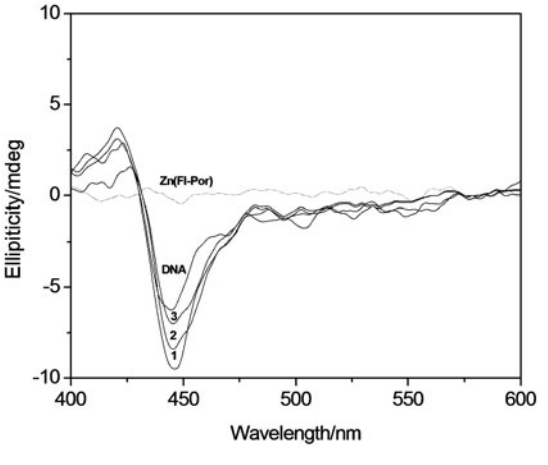

Figure 6. Induced CD spectra of **1**, **2** and **3** in the absence (…) and presence (—) of CT-DNA. [Zn(Fl-Por)] = 10 μML^{-1}, [DNA] = 120 μML^{-1}. The spectra were recorded at 25 °C after samples had been incubated with CT DNA for 24 h at 37 °C.

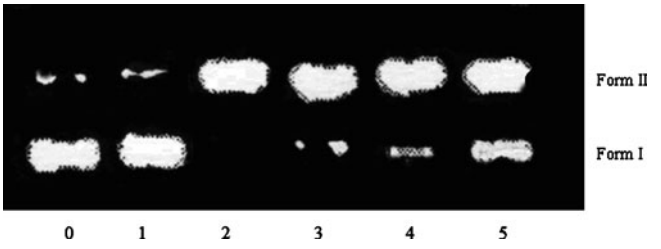

Figure 7. Photo-activated cleavage of pBR 322 DNA in the presence of **1**, **2** and **3** after 60 min irradiation at 365 nm. Lane 0, DNA alone; Lane 1, DNA + TPP (40 μML^{-1}); Lane 2, DNA + **1** (40 μML^{-1}); Lane 3, DNA + **2** (40 μML^{-1}); Lane 4, DNA + **3** (40 μML^{-1}); Lane 5, DNA + fluorescein (40 μML^{-1}).

electrophoresis, relatively fast migration will be observed for the intact supercoiled form (form I). If scission occurs on one strand (nicking), the supercoil will relax to generate a slower-moving open circular form (form II). If both strands are cleaved, a linear form (form III) migrating between forms I and II will be generated [32, 33, 36, 41].

The gel electrophoretic separations of plasmid pBR 322 DNA after incubation with fluorescein–porphyrinatozinc(II) complexes and irradiation with white-light (including 350 nm (fluorescein absorption) and 420 nm (porphyrin absorption, 25 mW cm^{-2})) are shown in figure 7. The gel electrophoretic pattern of plasmid pBR 322 DNA is after incubation with ZnTPP (TP*p* = 5,10,15,20-tetraphenylporphyrin), fluorescein or fluorescein–porphyrinatozinc (II) complexes (**1**, **2**, or **3**) and irradiation with white-light. No significant DNA cleavage was observed for negative controls (lane 0) and/or in the control experiment in which fluorescein-porphyrinatozinc(II) complex was replaced by ZnTPP (Lane 1). However, for **1**, **2,** and **3** (Lanes 2–4), at 40 μML^{-1}, significant amounts of the open circular form II were observed, indicating that these three complexes can cleave pBR 322 DNA efficiently. Under comparative experimental conditions, the cleavage ability follows the order **1** > **2** > **3**. Noticeably, for fluorescein (Lane 5), at 40 μML^{-1}, significant amounts of Form II were also visible, which implies that fluorescein–porphyrinatozinc(II) complexes bind to CT-DNA by intercalation via the plane of fluorescein into the base pairs of DNA [37, 42–44]. Further investigation is required to study the possible cleavage mechanisms of these three complexes.

3.4. *Cytotoxicity studies in vitro*

3.4.1. Cytotoxicity assays. The antitumor activities of these complexes against Ag8.653 and U251 cell lines were evaluated by MTT assay [4, 45–47]. The IC_{50} values obtained for the complexes against two tumor cell lines are shown in table 2. The synthetic

Table 2. The IC_{50} values for **1**, **2,** and **3** against Ag8.653 and U251 cell lines.[a]

Compounds	IC_{50} (μML^{-1}) Ag8.653	IC_{50} (μML^{-1}) U251
Cisplatin	0.002 ± 0.001	0.005 ± 0.001
1	0.896 ± 0.286	1.586 ± 0.279
2	1.187 ± 0.294	2.015 ± 0.268
3	1.530 ± 0.336	2.328 ± 0.423

[a]Cells were treated with various concentrations of tested compounds for 48 h. Cell viability was determined by MTT assay and IC50 values were calculated as described in Section 2. Each value represents the mean ± SD of three independent experiments.

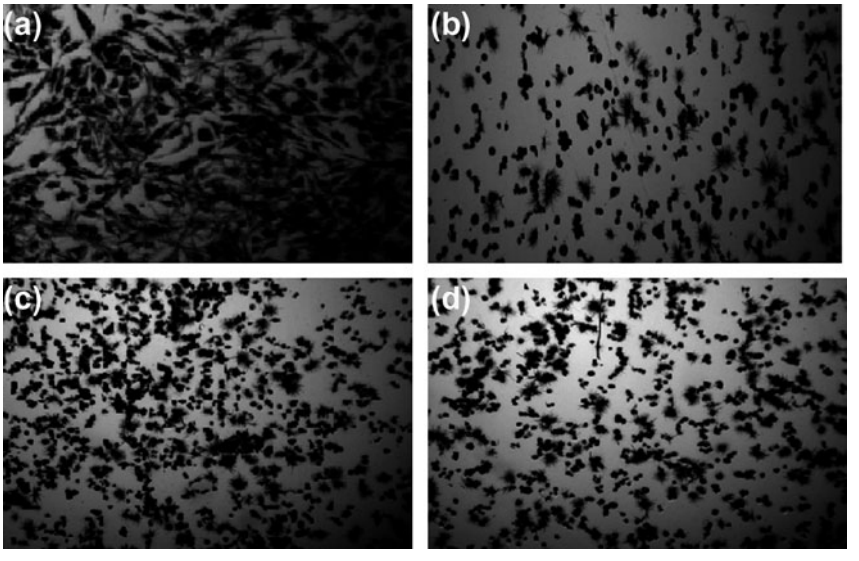

Figure 8. Micrograph of the myeloma tumor (Ag8.653) cell line after treatment for 48 h in the absence (a) (control) and presence of **1** (b), **2** (c) and **3** (d), respectively, [Zn(Fl-Por)] = 200 μML^{-1}. Cells were observed using an inverted microscope and photographed by a digital camera.

fluorescein–porphyrinatozinc(II) complexes exhibit broad inhibition on the two tested human cancer cell lines with IC_{50} values ranging from 0.996 to 2.328 μML^{-1}, respectively. The results also indicate that all of these fluorescein–porphyrinatozinc(II) complexes exhibit antitumor activities against the selected cell lines in different concentrations and antitumor activities are concentration-dependent [45, 46]. With comparison of the antitumor activities of cisplatin, fluorescein–porphyrinatozinc(II) complexes appeared to be less cytotoxic against the cell lines of Ag8.653 and U251. Figure 8 shows the antiproliferative activity in the absence (a) and presence of **1** (b), **2** (c), and **3** (d), at 200 μML^{-1}. It shows that the proliferation of tumor cells of Ag8.653 was effectively inhibited.

Complex **1** possessed the most potent inhibitory effect against the two cell lines. Its IC50 value, which is higher than that of cisplatin, indicated its high cytotoxic effects against human cancer cells. This is consistent with its binding abilities with CT-DNA, indicating that the antitumor abilities of the fluorescein–porphyrinatozinc(II) complexes may be closely related to their DNA binding mode.

3.4.2. Cell cycle analysis. In order to further define the mechanism of anti-proliferative effect of fluorescein–porphyrinatozinc(II) complexes on tumor cells, the cell cycle phase distribution was analyzed by flow cytometry with PI staining [47–49]. According to the results of table 3, Ag8.653 cells exhibited the highest sensitivity to **1**. Thus, this cell line was used for further investigation on the underlying mechanisms accounting for the antiproliferative action. The Ag8.653 cells were treated with 0.001, 0.002, and 0.004 μML^{-1} of **1** for 48 h, respectively. As shown in table 3, the G2/M phase was arrested significantly after Ag8.653 cells were exposed to 0.004 μM (IC_{50} values) of **1** for 48 h. Treatment with 0.001 or 0.002 μML^{-1} of **1** resulted in modest G2/M phase arrest of Ag8.653 cells at 48 h. The results in this work showed significantly decreased G0/G1

Table 3. The cell cycle analysis of the Ag8.653 cells induced by **1**.

Concentration (μML^{-1})	The relative proportion of different phased in the cell cycle (%)			
	G0/G1	G2/M	S	APO
Control	68.26 ± 3.47	9.50 ± 0.66	20.56 ± 3.40	0.39 ± 0.26
0.001	60.00 ± 3.73*	14.07 ± 0.75**	19.92 ± 1.77	3.98 ± 1.78*
0.002	50.10 ± 3.54**	18.87 ± 2.83**	20.45 ± 2.13	4.35 ± 1.80**
0.004	41.93 ± 1.76**	22.32 ± 3.68**	19.61 ± 2.79	6.25 ± 1.87**

Notes: Data are the mean ± SD of at least three independent experiments. $^{*}p < 0.05$; $^{**}p < 0.01$.$^{*}p < 0.05$ *vs.* the control, the difference was significant. $^{**}p < 0.01$ *vs.* the control, the difference was markedly significant.

phase distribution and increased G2/M phase distribution in a dose-dependent manner, indicating induction of G0/G1-phase arrest by **1**. Moreover, apoptotic cells and cell debris significantly increased after Ag8.653 cells were exposed to **1**. The results suggested that fluorescein–porphyrinatozinc(II) complexes induced proliferative suppression of Ag8.653 cells were via the induction of apoptosis [4, 45, 48–51]. To fully understand the mechanism involved in the induction of apoptosis by fluorescein–porphyrinatozinc(II) complexes, further investigation will be need to be carried out.

4. Conclusions

Three fluorescein–porphyrinatozinc complexes Zn(Fl-PPTPP) (**1**), Zn(Fl-HPTPP) (**2**), and Zn(Fl-DPTPP) (**3**) were synthesized and characterized. The interactions of these three complexes with CT-DNA were studied using UV/Vis, fluorescence spectroscopic titration, viscosity measurements, thermal denaturation and CD. The results suggest that **1**, **2,** and **3** interact with CT-DNA by intercalative modes. The DNA-binding affinity, K_b values follows the order **1** > **2** > **3**. Their photocleavage reactions with pBR322 supercoiled plasmid DNA were investigated. All of the complexes exhibit significant DNA cleavage activity, and the cleavage ability also follows the order **1** > **2** > **3**, which is in parallel with the magnitude of their intrinsic binding constants, K_b values. The results also suggest that fluorescein–porphyrinatozinc(II) complexes bind to CT-DNA by intercalation via the planar fluorescein into the base pairs of DNA, and the conformation of fluorescein–porphyrin hybrids is an important factor affecting the DNA binding affinities of these complexes. The results may be helpful in better understanding the interactions between DNA and metallo-porphyrins. In addition, these complexes present cytotoxic activities against Ag8.653 and U251 cell lines and suggest that porphyrinatozinc complexes may have utility in chemoprevention of human cancers.

Conflict of interest

The authors have declared that there is no conflict of interest.

Abbreviations

MTT	3-(4,5-dimethylthiazoyl-2-yl)-2,5-diphenyltetrazoliumbromide
IC_{50}	50% inhibition concentrations
Tm	the DNA-melting temperature where total base pairs are unbound
ES-MS	electrospray mass spectra
TPP	5,10,15,20-tetraphenylporphyrin
CT-DNA	calf thymus DNA

Tris	tris(hydroxymethyl)aminomethane
DMF	N,N-Dimethyformamide
DMSO	dimethyl sulfoxide
EDTA	N, N′-1,2-Ethanediylbis[N-(carboxymethyl)]glycine
PBS	Phosphate Buffer Solution
PI	Propidium Iodide
RPMI	SeraFree Cryopreservation Media

Acknowledgments

We gratefully acknowledge financial support for this work by the Science and Technology Research Project of Guangdong Province, P.R. China (No. 2012B031800431), the National Key Research Project of China (No. 2011zx09102-001-31) and the National Natural Science Foundation of P.R. China (Nos. 21101033 and 81102753).

References

[1] M.G. Vicente. *Anti Cancer Agents*, **1**, 175 (2001).
[2] N.L. Oleinick, H.H. Evans. *Radiat. Res.*, **150**, 146 (1998).
[3] K. Lang, J. Mosinger, D.M. Wagnerova. *Coord. Chem. Rev.*, **248**, 321 (2004).
[4] T.J. Jensen, M.G.H. Vicente, R. Luguya, J. Norton, F.R. Fronczek, K.M. Smith. *J. Photochem. Photobiol., B*, **100**, 100 (2010).
[5] Y.B. Dalyan, S.G. Haroutiunian, G.V. Ananyan, V.I. Vardanyan, D.Y. Lando, V.N. Madakyan, R.K. Kazaryan, L. Messory, P.L. Orioli, A.S. Benight. *J. Biomol. Struct. Dyn.*, **18**, 677 (2001).
[6] G.M. Gelfuso, T. Gratieri, J.G. Souza, J.A. Thomazine, R.F.V. Lopez. *Eur. J. Pharm. Biopharm.*, **77**, 249 (2011).
[7] L.A. Lipscomb, F.X. Zhou, S.R. Presnell, R.J. Woo, M.E. Peek, R.R. Plaskon, L.D. Williams. *Biochemistry*, **35**, 2818 (1996).
[8] G. Raner, B. Ward, J.C. Dabrowiak. *J. Coord. Chem.*, **19**, 17 (1988).
[9] B.H. Yun, S.H. Jeon, T.S. Cho, S.Y. Yi, U. Sehlstedt, S.K. Kim. *Biophys. Chem.*, **70**, 1 (1998).
[10] D.R. McMillin, A.H. Shelton, S.A. Bejune, P.E. Fanwick, R.K. Wall. *Coord. Chem. Rev.*, **249**, 1451 (2005).
[11] R.F. Pasternack. *Chirality*, **15**, 329 (2003).
[12] B. Jin, J.S. Shin, C.H. Bae, J.M. Kim, S.K. Kim. *Biochem. Biophys.*, **1760**, 993 (2006).
[13] H. Gong, C.Q. Cai, Y. Ma, X.M. Chen. *Microchim. Acta*, **177**, 95 (2012).
[14] S.A.A. Sulyman, A.A. Ghazaryan, Y.B. Dalyan. *Armenian J. Phys.*, **2**, 139 (2009).
[15] R. Kuroda, E. Takahashi, C.A. Austin, L.M. Fisher. *FEBS Lett.*, **262**, 293 (1990).
[16] P. Zhao, L.C. Xu, J.W. Huang, J. Liu, H.C. Yu, L.N. Ji. *Spectrochim. Acta, Part A*, **71**, 1216 (2008).
[17] Y.K. Kang, P.M. Iovine, M.J. Therien. *Coord. Chem. Rev.*, **255**, 804 (2011).
[18] H. Yanga, K.L. Meterab, H.F. Sleiman. *Coord. Chem. Rev.*, **254**, 2403 (2010).
[19] X.B. Yan, M. Weng, M.H. Zhang, T. Shen. *Dyes Pigm.*, **36**, 259 (1998).
[20] J.Z. Lu, Y.F. Du, B. Wu, J.W. Huang, J. Jiang. *Transition Met. Chem.*, **35**, 451 (2010).
[21] J.Z. Lu, J.W. Huang, L.F. Fan, J. Liu, X.L. Chen, L.N. Ji. *Inorg. Chem. Commun.*, **7**, 1030 (2004).
[22] J.Z. Lu, X.C. Tan, J.W. Huang, C.H. Dong, L.N. Ji. *Transition Met. Chem.*, **30**, 643 (2005).
[23] J.Z. Lu, H.W. Guo, Y.L. Zhang, J. Jiang, Y.J. Liu, L.Q. Zang, J.W. Huang. *J. Coord. Chem.*, **65**, 1765 (2012).
[24] P. Zhao, L.C. Xu, J.W. Huang, B. Fu, H.C. Yu, L.N. Ji. *Bioorg. Chem.*, **36**, 278 (2008).
[25] J.Z. Lu, Y.F. Du, H.W. Guo. *J. Coord. Chem.*, **64**, 1229 (2011).
[26] Y.F. Du, J.Z. Lu, H.W. Guo, J. Jiang. *Transition Met. Chem.*, **35**, 859 (2010).
[27] S. Tuncer, A. Koca, A. Gul, U. Avcata. *Dyes Pigm.*, **81**, 144 (2009).
[28] M. Fujita, S. Nagao, K. Ogura. *J. Am. Chem. Soc.*, **117**, 1649 (1995).
[29] S.J. Wezenberg, G.A. Metselaar, E.C. Escudero-Adán, J.B. Buchholz, A.W. Kleij. *Inorg. Chim. Acta*, **362**, 1053 (2009).
[30] G. Ananyan, A. Avetisyan, L. Aloyan, Y. Dalyan. *Biophys. Chem.*, **156**, 96 (2011).
[31] J.A. Strickland, L.G. Marzilli, K.M. Gay, W.D. Wilson. *Biochemistry*, **27**, 8870 (1988).
[32] H.L. Wu, Y. Bai, J.K. Yuan, H. Wang, G.L. Pan, X.Y. Fan, J. Kong. *J. Coord. Chem.*, **65**, 2839 (2012).
[33] J. Qian, L.P. Wang, W. Gu, X. Liu, J.L. Tian, S.P. Yan. *J. Coord. Chem.*, **64**, 2480 (2011).

[34] W.K. Dong, S.J. Xing, Y.X. Sun, L. Zhao, L.Q. Chai, X.H. Gao. *J. Coord. Chem.*, **65**, 1212 (2012).
[35] M. Bennett, A. Krah, F. Wien, E. Garman, R. Mckenna, M. Sanderson, S. Niedle. *Proc. Nat. Acad. Sci. USA*, **97**, 9476 (2000).
[36] A. McCrate, M. Carlone, M. Nielsen, S. Swavey. *Inorg. Chem. Commun.*, **13**, 537 (2010).
[37] E. Craver, A. McCrate, M. Nielsen, S. Swavey. *Inorg. Chim. Acta*, **363**, 453 (2010).
[38] Z. Xu, S. Swavey. *Inorg. Chem. Commun.*, **14**, 882 (2011).
[39] G. Mező, L. Herényi, J. Habdas, Z. Majer, B. Myśliwa-Kurdziel, K. Tóth, G. Csík. *Biophys. Chem.*, **155**, 36 (2011).
[40] S. Lee, S.H. Jeon, B.J. Kim, S.W. Han, H.G. Jang, S.K. Kim. *Biophys. Chem.*, **92**, 35 (2001).
[41] F. Arjmand, F. Sayeed, M. Muddassir. *J. Photochem. Photobiol., B*, **103**, 166 (2011).
[42] T.F. Al-Azemi, M. Vinodh. *Tetrahedron*, **67**, 2585 (2011).
[43] J.K. Barton, A.L. Raphael. *J. Am. Chem. Soc.*, **106**, 2466 (1984).
[44] B.E. Smith, T.D. Lash. *Tetrahedron*, **66**, 4413 (2010).
[45] J.N. Silva, A. Galmiche, J.P.C. Tome, A. Boullier, M.G.P.M.S. Neves, E.M.P. Silva, J.C. Capiod, J.A.S.C. Rene Santus, J.C. Mazie, P. Filipe, P. Morlie. *Biochem. Pharmacol.*, **80**, 1373 (2010).
[46] V. Vaz Serra, A. Zamarrón, M.A.F. Faustino, M.C.I. Cruz, A. Blázquez, J.M.M. Rodrigues, M.G.P.M.S. Neves, J.A.S. Cavaleiro, A. Juarranz, F. Sanz-Rodríguez. *Bioorg. Med. Chem.*, **18**, 6170 (2010).
[47] Y. Liu, T.F. Chen, Y.S. Wong, W.J. Mei, X.M. Huang, F. Yang, J. Liu, W.J. Zheng. *Chem. Biol. Interact.*, **183**, 349 (2010).
[48] C.T. Luma, X. Liu, R.W.Y. Sun, X.P. Li, Y. Peng, M.L. He, H.F. Kung, C.M. Che, M.C.M. Lin. *Cancer Lett.*, **294**, 159 (2010).
[49] R. Kim. *Cancer*, **103**, 1551 (2005).
[50] R.S. Ray, B. Rana, B. Swami, V. Venu, M. Chatterjee. *Chem. Biol. Interact.*, **163**, 239 (2006).
[51] I. Kostova. *Anticancer Agents Med. Chem.*, **9**, 827 (2009).